

Technical Note: Rapid multiexponential curve fitting algorithm for voxel-based targeted radionuclide dosimetry

Price Jackson^{a)}

*Department of Molecular Imaging & Therapeutic Nuclear Medicine, Peter MacCallum Cancer Centre, Melbourne 3000, Australia
Sir Peter MacCallum Department of Oncology, University of Melbourne, Melbourne 3010, Australia*

Lachlan McIntosh

Department of Molecular Imaging & Therapeutic Nuclear Medicine, Peter MacCallum Cancer Centre, Melbourne 3000, Australia

Michael S. Hofman, Grace Kong, and Rodney J. Hicks

*Department of Molecular Imaging & Therapeutic Nuclear Medicine, Peter MacCallum Cancer Centre, Melbourne 3000, Australia
Sir Peter MacCallum Department of Oncology, University of Melbourne, Melbourne 3010, Australia*

(Received 21 November 2019; revised 24 April 2020; accepted for publication 11 May 2020; published 12 June 2020)

Background: Dosimetry in nuclear medicine often relies on estimating pharmacokinetics based on sparse temporal data. As analysis methods move toward image-based three-dimensional computation, it becomes important to interpolate and extrapolate these data without requiring manual intervention; that is, in a manner that is highly efficient and reproducible. Iterative least-squares solvers are poorly suited to this task because of the computational overhead and potential to optimize to local minima without applying tight constraints at the outset.

Methodology: This work describes a fully analytical method for solving three-phase exponential time-activity curves based on three measured time points in a manner that may be readily employed by image-based dosimetry tools. The methodology uses a series of conditional statements and a piecewise approach for solving exponential slope directly through measured values in most instances. The proposed algorithm is tested against a purpose-designed iterative fitting technique and linear piecewise method followed by single exponential in a cohort of ten patients receiving ¹⁷⁷Lu-DOTA-Octreotate therapy.

Results: Tri-exponential time-integrated values are shown to be comparable to previously published methods with an average difference between organs when computed at the voxel level of $9.8 \pm 14.2\%$ and $-3.6 \pm 10.4\%$ compared to iterative and interpolated methods, respectively. Of the three methods, the proposed tri-exponential algorithm was most consistent when regional time-integrated activity was evaluated at both voxel- and whole-organ levels. For whole-body SPECT imaging, it is possible to compute 3D time-integrated activity maps in <5 min processing time. Furthermore, the technique is able to predictably and reproducibly handle artefactual measurements due to noise or spatial misalignment over multiple image times.

Conclusions: An efficient, analytical algorithm for solving multiphase exponential pharmacokinetics is reported. The method may be readily incorporated into voxel-dose routines by combining with widely available image registration and radiation transport tools. © 2020 American Association of Physicists in Medicine [https://doi.org/10.1002/mp.14243]

Key words: image processing, pharmacokinetics, radionuclide dosimetry

1. BACKGROUND

Driven by increasing recognition of the clinical benefits of radionuclide therapy particularly in neuroendocrine tumors and prostate cancer,^{1,2} Image-based dosimetry in nuclear medicine has been a focus of physics and computational development. The MIRD committee has published coefficients for estimating radiation transport from sources at the voxel level³ and other groups have supplemented these tables for a variety of cubic dimensions and common therapeutic isotopes.^{4,5} This has been extended to patient-specific Monte Carlo calculations which may now be performed in a clinically achievable timeframe.^{6,7} There has been consideration of the spatial effects of ionization relative to source location

with respect to the resolution of the imaging systems used to infer that source distribution.⁸ There has also been work extending dose metrics to infer radiobiological effect according to dose-rate and spatial heterogeneity.⁹

While much focus has been applied to computation of radiation physics, research in pharmacokinetic interpolation is relatively limited. Inferring the input time-integrated activity map — a three-dimensional (3D) grid of the number of disintegrations per voxel — represents a comparably challenging task both in terms of complexity and potential to introduce errors in the predicted dose-volume. In the ideal instance this is performed entirely in the image space allowing dosimetry to be appreciated at the level of detail attained by a SPECT imaging system. Typically this workflow

involves serial acquisition of multiple quantitative SPECT images¹⁰ with pharmacokinetic time-activity curves (TACs) derived independently for each position in the aligned image sequence.¹¹

One of the primary challenges in computing voxelized TACs is employing a routine that is generalizable — that is one that can be applied uniformly throughout the variety of tissues in the body — while operating without manual oversight and at minimal concession to fitting accuracy. Sarrut *et al.*¹² described an algorithm that places voxels into different classes to simplify the optimization challenge and penalize models based on their complexity. This in principle yields more reproducible results than an unconstrained least-squares method. A similar approach had previously been employed by Kletting *et al.* to enable users to designate between a variety of fitting functions based on the shape of pharmacokinetic measurements, however, in requiring user input would not be appropriate for voxel-level dose estimation.¹³ In this work a general three-phase exponential model is applied which offers the flexibility to characterize components of uptake as well as a mixture of slow and fast tissue clearance components.

An analytical pharmacokinetic estimation technique is reported in detail including the sequence of computational operations and methods for handling noisy or otherwise irregular data. The technique provides the basis for a previously published voxel dosimetry software package¹⁴ and has been shown to be reliable across a variety of clinical trial datasets.¹⁵ Given that all phases of the pharmacokinetic curves — even those of uptake — may be described by equations of exponential decay it is possible to approach the problem as a piecewise operation. By solving for the slope between the final two measurements the preceding phases can be solved in sequence moving to earlier times based on the difference between measured values and the trajectory of the previously predicted phase as a simplified curve-stripping process.¹⁶ Depending on the data conditions, where measurement values lie within respective reference lines, the most appropriate order of solving may vary. In some instances, for example when activity continues to increase beyond the second image time, the curve is best approximated by only two phases using sustained uptake from injection to the final measurement followed by physical decay in the period beyond. This facilitates simplification of a highly unconstrained problem — six variables with only three data points — using only a few straightforward assumptions and computational logic operations. With judicious selection of acquisition times this form of curve generation may be applied in a manner that is representative and without systematic bias for a wide variety of pharmacokinetic models.

2. MATERIALS AND METHODS

With the aim to solve parameters that define a three-phase exponential curve described by Eq. (1), A_{1-3}/k_{1-3} the ideal case includes a single phase of tissue uptake and up to two phases of clearance. This model may describe periods of

rapid washout and long-term retention; each with a variable half-life and relative proportion as represented across a variety of pharmacokinetic tissue types.

$$\text{Region Activity} = A_1 e^{k_1 t} + A_2 e^{k_2 t} + A_3 e^{k_3 t} \quad (1)$$

Three activity concentration values are described as c_{1-3} and time points as t_{1-3} . As a preliminary step, the convention is taken to decay correct all image data, $c_{i1-3} \rightarrow c_{1-3}$, as illustrated in Fig. 1. This handles concentration values in pharmacological terms during fitting. The decay correction is straightforward to reverse when taking the final integral calculation and offers practical advantage to ensure that the pharmacological concentration does not continue to increase beyond the final imaging time point. This should be a reasonable assumption given judicious selection of imaging time points.¹⁷ Specifically, it prevents the final integral from exceeding a value that would exceed the physical half-life of the isotope; curves which deplete more slowly than the half-life of the radionuclide. If the highest activity measurement is detected at the final time point, fitting a slope very near zero, $k_3 \approx -\infty$, equates to only physical decay. Secondly, this provides a simple mechanism to adapt the algorithm for other isotope or diagnostic/therapeutic pairs, for example using sequential ^{124}I PET/CT imaging to predict radiation dose from ^{131}I radioactive iodine. The user only needs to provide the physical half-life of each tracer and the same algorithm may be applied to compute local time-integrated activity concentration (decays per unit volume) for the given quantity of activity administered.

The ideal case can be described by a transient uptake phase between $t = 0$ and t_1 followed by distinct periods of rapid and delayed washout in the t_{1-2} and t_{2-3} time spans, respectively, as shown in Fig. 2. In clinical use of long half-life therapeutic isotopes, after initial uptake, one or two exponential clearance phases of activity from organs and tumors are widely

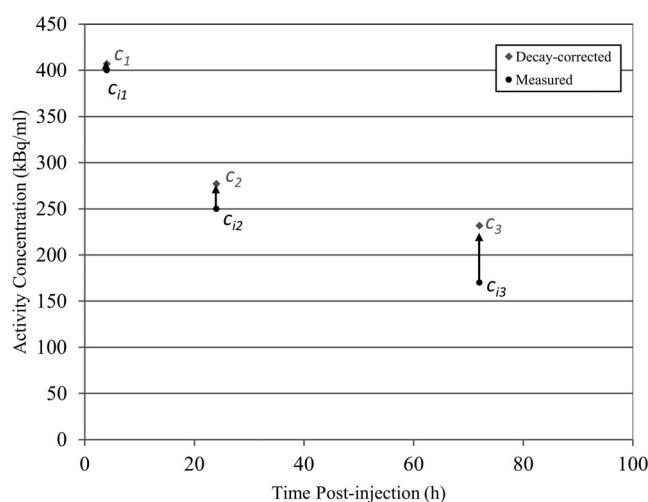


FIG. 1. Decay-correcting initial measured data before fitting ensures algorithm does not fit increasing pharmacological concentration beyond final imaging time point. This is accounted for when calculating time-integrated activity and easily permits estimates from diagnostic/therapeutic isotope pairs such as $^{124}\text{I}/^{131}\text{I}$.

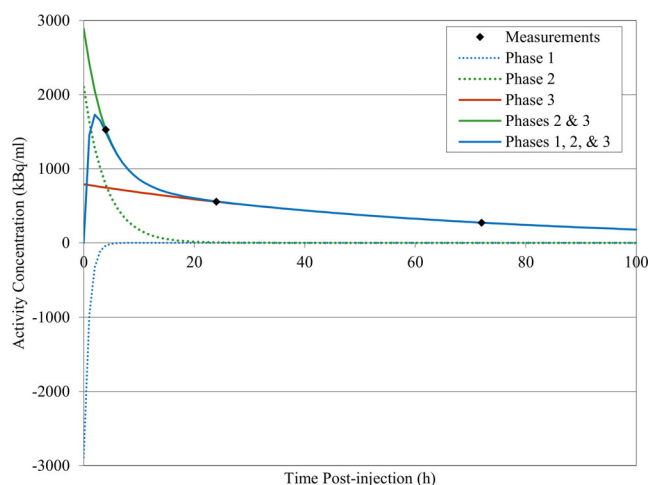


FIG. 2. Illustration of typical time-activity curve comprised of three exponential phases that has been solved to pass through measured data points. Plots of the component exponential curves, one uptake and two clearances, are shown as dashed lines. The sum of phases 2 and 3 and all phases are shown as solid green and solid blue, respectively. Note that phase 1 and phase 2 effectively deplete as the curve nears measurement time points 1 and 2. [Color figure can be viewed at wileyonlinelibrary.com]

described.¹⁸ It is possible to fit a curve of exponential decay between two points as shown in Fig. 3 with the form:

$$A = A_0 e^{kt} \quad (2)$$

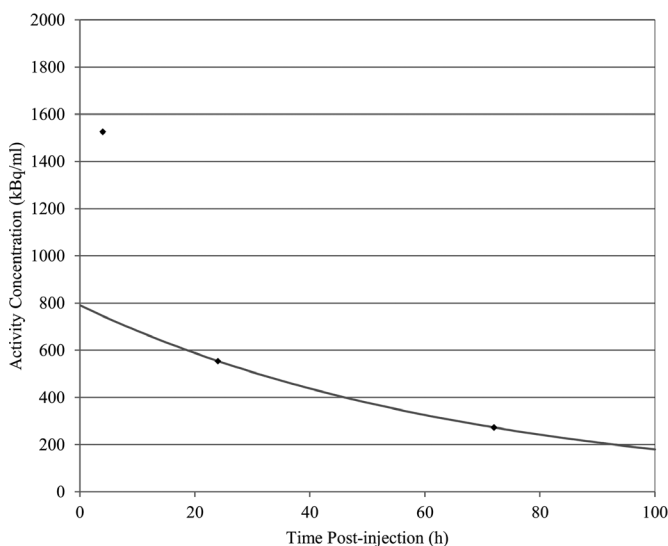
Solving for the linear fit, $y = mx + b$, by log transform of the activity values starting with the final phase, the kinetic parameter, k_3 , is determined by:

$$k_3 = m = \frac{\ln(c_3) - \ln(c_2)}{t_3 - t_2} \quad (3)$$

and the amplitude parameter, A_3 , is then:

$$A_3 = e^b = e^{\ln(c_2) - k_3 t_2} \quad (4)$$

As a first instance, this method provides the slope of the line representing the long-term retention phase. The



preceding phase can be described as the difference between the slope described by the A_3, k_3 curve and the value at c_1 using another exponential decay equation that depletes as it approaches t_2 . This very nearly builds a piecewise function from exponential terms. Solving by log transform requires nonzero values, so, for simplicity, we adjust the latter activity value, Δc_2 , to be in the range of 1–3% of the measured value c_2 . Some discussion of the special conditions which warrant the variability is provided in later sections. The process may be more clearly illustrated by the mixture of curves in Fig. 4. The residual of the curve, Δc_1 , is the difference between the slope of the late phase and the first measured activity value, c_1 :

$$\Delta c_1 = c_1 - A_3 e^{k_3 t_1} \quad (5)$$

The sign of the delta value is evaluated: $\Delta c_2 = 0.01 * c_2$ if Δc_1 is greater than zero. If not, the sign is reversed to $\Delta c_2 = -0.01 * c_2$. That is, both delta values should be positive or negative. There are conditions when a negative A_2 provides the most appropriate fit based on the measured data. Curve approximation then follows the previous method of solving for exponential slope to generate a phase that depletes as it approaches c_2 :

$$k_2 = \frac{\ln(\Delta c_2) - \ln(\Delta c_1)}{t_2 - t_1} \quad (6)$$

$$A_2 = e^{\ln(\Delta c_1) - k_2 t_1}$$

Estimating the very early uptake kinetics requires an approximation when there are no intermediate points before the peak activity measurement. This is typical when only one image is available during the first day of administration. One approach is to infer the uptake pharmacokinetics based on a generic rate constant, k_1 . For long half-life therapeutic isotopes, the majority of the time-integrated activity calculation is dictated by the late-phase retention. That is, if the physical half-life is several days or longer, only select tissues with significant initial uptake followed by rapid and sustained

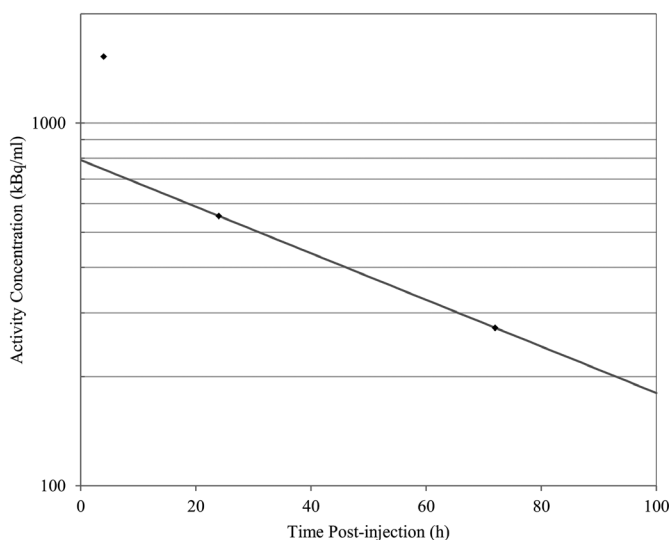


FIG. 3. Standard (left) and logarithmic (right) plots of method to solve late-phase clearance based on exponential slope between measurement time points 2 and 3.

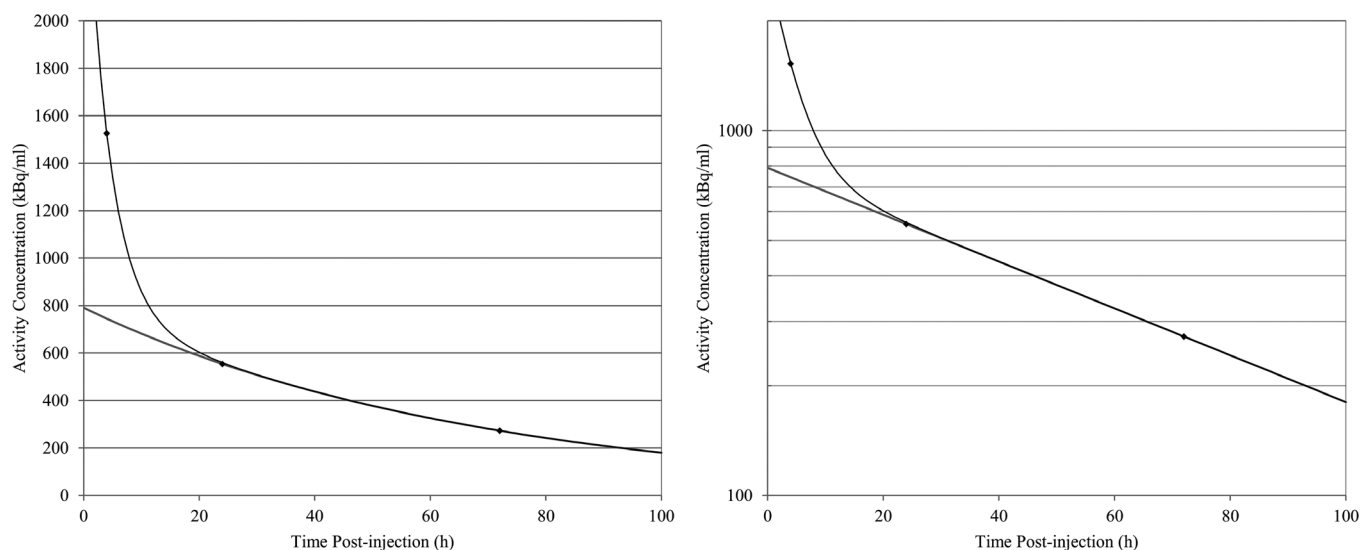


FIG. 4. Method to solve phase 2, first clearance phase, based on the difference in the curve described by Fig. 2 and the measured activity at time point 1. Standard (left) and logarithmic (right) plots are shown to illustrate piecewise nature of the individual curve phases.

clearance could be appreciably impacted by the use of a generic uptake parameter. The notable exception is choosing a small k_1 parameter representing very rapid uptake. In this case, the presented algorithm may yield a curve that escalates dramatically at times close to $t = 0$ due to the nature of solving the line-of-fit for the fast clearance phase. With ^{177}Lu , a half-time of approximately 30 min, $k_1 = -1.3$, has been shown to offer reasonable agreement with other curve fitting integrals over a range of different tissue types.^{14,19} An analysis of the influence of the generic rate parameter on time-integrated activity is provided in Table I showing that over a range of half-times from 20 to 90 min, the effect is in the order of $\pm 2\%$ except in bladder and heart (blood pool). Finally, the amplitude, A_1 , of the uptake phase is set such that concentration value passes through zero at $t = 0$. Here the term A_1 becomes the negative of the sum of A_2 and A_3 .

In this manner, it is possible to analytically solve a three-phase exponential that very closely passes through three measured time points. This piecewise method, or a slightly modified version, can be applied wherever declining slope is detected between values of c_2 and c_3 ; that is, whenever some clearance is detected in the late phase of imaging as would be typical of most tracers and tissue types. The sequence of computations is depicted in the flowchart shown by Fig. 6 with this common case designated by bold labels.

With the solved time-activity curve, it is then possible to integrate the decay-corrected curve from $t_0 \rightarrow \infty$ including the physical half-life of the isotope in the form:

$$\tilde{A} = \frac{A_1}{\left(\frac{\ln 2}{t_{1/2}} + k_1\right)} + \frac{A_2}{\left(\frac{\ln 2}{t_{1/2}} + k_2\right)} + \frac{A_3}{\left(\frac{\ln 2}{t_{1/2}} + k_3\right)} \quad (7)$$

where \tilde{A} is the time-integrated activity or total number of disintegrations in the region described by the time-activity curve, $t_{1/2}$ is the physical half-life of the therapeutic isotope,

and the parameters A_{1-3} and k_{1-3} are the fitting values described previously.

A detailed explanation of conditional methods to derive curves for irregular, or slowly accumulating data is provided in the Figs. S1–S3). This involves methods to classify the shape of the curve to apply algorithmic steps suited to that pharmacokinetic type. In some instances, such as when activity decreases from c_1 to c_2 and increases again at c_3 the algorithm will interpolate an intermediate location to analytically define a curve that balances the necessary error between measurements with a behavior that is similar to least-squares optimization. It is worth noting that for these cases, the convention is taken to define a curve that as often as possible passes directly through the final measurement time — typically the most important for long half-life isotopes — and subsequently mitigate the error for the line-of-fit that passes through or near the preceding times. Flowcharts to illustrate the conditional sequence of processing are given in Figs. S4–S6.

The multiexponential algorithm was tested in clinical application in a representative cohort of ten patients receiving ^{177}Lu -DOTA-Octreotate. Cases were followed up by serial post-treatment quantitative SPECT imaging at timelines of 4, 24, and 72 h. Pharmacokinetics were then computed at the voxel level with the proposed tri-exponential algorithm. For comparison to two reference methodologies, time-integrated activity was estimated by piecewise linear approximation between image times followed by a single-exponential phase determined by the effective half-life over the final two image acquisitions.²⁰ In voxels where the detected clearance rate was slower than the physical half-life of ^{177}Lu , clearance was instead based on physical decay. Secondly, the iterative fitting technique described by Sarrut et al., the voxel-based multimodal method (VoMM), was implemented with Python libraries.^{12,21} In that method, iterative optimization is

TABLE I. Estimated time-integrated activity for representative cohort of ^{177}Lu -DOTA-Octreotate therapies as computed using proposed tri-exponential algorithm, voxel-based multimodal, and simplified piecewise with single late-phase exponential methods. Results are provided based on curves computed at the voxel level (mean of all curves) and additionally based on a single curve for each organ using the mean activity concentration at each time point.

| | Mean time-integrated activity concentration (MBq*h/ml) | | | | | |
|-----------------------|--|--------|--------------------------------|-----------------|--------|--------------------------------|
| | Voxel level | | | Whole organ | | |
| | Tri-exponential | VoMM | Trapezoid + single exponential | Tri-exponential | VoMM | Trapezoid + single exponential |
| Marrow | 2.78 | 2.52 | 2.95 | 2.78 | 2.86 | 2.88 |
| Muscle | 1.21 | 1.22 | 1.28 | 1.03 | 1.06 | 1.05 |
| Lung | 1.01 | 1.04 | 1.11 | 0.95 | 0.96 | 1.04 |
| Heart | 1.62 | 1.71 | 1.76 | 1.54 | 1.62 | 1.64 |
| Stomach | 14.92 | 13.86 | 15.57 | 14.03 | 13.51 | 14.39 |
| Small bowel | 3.51 | 3.32 | 3.65 | 2.93 | 2.97 | 2.93 |
| Liver | 27.46 | 24.96 | 27.98 | 26.53 | 26.74 | 26.08 |
| Pancreas | 17.53 | 15.04 | 18.64 | 18.02 | 16.20 | 19.18 |
| Spleen | 56.26 | 52.05 | 57.64 | 53.43 | 53.82 | 52.54 |
| Right kidney | 39.27 | 35.96 | 40.16 | 36.97 | 37.51 | 36.86 |
| Left kidney | 35.88 | 32.61 | 36.38 | 33.99 | 34.88 | 33.98 |
| Bladder | 20.23 | 25.33 | 34.65 | 18.99 | 24.81 | 33.13 |
| Lower large intestine | 10.92 | 7.40 | 10.85 | 10.41 | 7.79 | 10.28 |
| Upper large intestine | 5.35 | 4.96 | 5.14 | 4.83 | 4.22 | 4.55 |
| Tumor | 327.83 | 290.79 | 345.99 | 330.26 | 347.25 | 351.85 |

performed for each voxel according to four different single- or multiexponential models and the most accurate line-of-fit with a penalty for model complexity is chosen. The resulting time-integrated activity concentration for each technique was compared both at the voxel level and based on a single curve derived from the mean activity in each volume-of-interest. For tumor and a selection of relevant tissues (kidney, spleen, liver, bladder, marrow, etc) time-integrated activity was assessed. Additionally the mean absolute error as weighted for voxel activity in predicted curves with the tri-exponential algorithm and VoMM method was investigated for each imaging time point. The median of all cases with each technique is summarized.

3. RESULTS

This work presents a computationally efficient methodology to solve highly unconstrained curve fitting in a predictable manner. The authors have previously demonstrated that this algorithm yields comparable regional dosimetry when applied independently across regional voxels to whole-organ methods employed with OLINDA coupled with a traditional iterative curve solver.^{14,19} In comparison to alternative voxel methods including trapezoidal interpolation followed by a single exponential and the previously published VoMM iterative technique, closest agreement between methods was observed in long-retaining tissues. Time-integrated activity in high-uptake organs (kidney, liver, spleen) — those considered at-risk in ^{177}Lu -Octreotate therapy — was on average within 10% for all curve fitting methods evaluated at the voxel level. Results for the ten patient cohort

are summarized in Table I and an evaluation of median voxel-wise fitting error at each of the three imaging time points is reported for the tri-exponential and VoMM techniques in Table II. The three methods were observed to be in closer agreement when pharmacokinetics were computed at the organ- rather than voxel level where the tri-exponential algorithm was within 5% of the VoMM technique for all regions except for bladder, intestines, and pancreas. Of the three, the proposed tri-exponential algorithm most closely reproduces the whole-organ time-integrated activity result when calculated from independent voxel curves with the lowest variation observed for 8 of the 15 regions including tumor, marrow, liver, and left kidney.

In comparison to a trapezoidal interpolation followed by single-exponential model, the multiexponential model was typically 3.5% lower in terms of estimated integral decays with most organs in the range of -1 to -8% . Much of the area under the curve for these therapies is dictated by the late-phase retention which should be similar in most cases with single- and tri-exponential evaluations. A significant difference in dose to bladder is reported with all three methods which may be attributed to the relative variation in uptake between images on the first day of therapy and those acquired at 24 h and beyond. Where tissues displaying this form of clearance are relevant for assessing potential toxicity, it is advisable to collect finer temporal sampling in the first day postadministration.

The scripted implementation of the fitting algorithm using Python computes at a rate of approximately 5000 voxels per second with clinical image data.^{14,22} Applying a condition to ignore background voxels — those with very low activity

values — dose volumes for a multibed SPECT series at 3.0 mm cubic spatial resolution can be computed in <5 min. Processing times were comparable to trapezoidal and single-exponential model. The iterative VoMM method was considerably more computationally intensive, previously reported at 800 voxels per second,¹² however, the python-based implementation would not be practical to apply across the full image space and voxel-wise fitting was restricted to labeled subregions. Image-based pharmacokinetics processing is often coupled with nonrigid image registration to tightly fuse the serial time points across the image volume.²³ That step will typically be equally or more computationally intensive than the pharmacokinetics process described in this work and as such this method of pharmacokinetic interpolation should not be considered a significant bottleneck to clinical workflows. As a complete image-based dosimetry tool, the algorithm has been employed in a variety of clinical studies for both therapeutic and diagnostic dose evaluation which have been used to inform patient management.^{24–27}

The overall residual error was observed to be comparable between iteratively optimized and tri-exponential algorithms, however, the VoMM method was shown to be most accurate at the early image phase with increasing error at later time points. This is to be anticipated as the observed activity — and potential to influence sum of squared error — carries less weight for the optimization task. In contrast, the proposed tri-exponential algorithm is designed to fit directly through the second and third measurements wherever the shape of the curve would sensibly permit. This may necessarily come at the sacrifice of accuracy in the very early phases; for example, in bowel which can be slow to accumulate ¹⁷⁷Lu-Octreotate over several days.

4. DISCUSSION

This work aims to describe an automated, reproducible, and efficient methodology for solving a large volume of time-activity curves with application to nuclear medicine dosimetry. The choice of three-phase exponential model affords the flexibility to characterize periods of tracer uptake as well as mixtures of slow- and fast clearance. By considering the sequence of operations, it is possible to address model overcomplexity: solving the most important phase at the outset and applying additional phases as necessary with decreasing influence on the time integral. The resulting algorithm is designed to yield comparable estimates of time-integrated activity to traditional methods including linear piecewise interpolation or constrained least-squares optimization. Additionally as a pure exponential model, it is straightforward to apply isotope decay corrections and integral calculations. Many of the standard kinetic coefficients selected in the present implementation are chosen empirically as a practical solution for use in ¹⁷⁷Lu-DOTA-octreotate dosimetry and with imaging times routinely used in clinical practice. The conditional methods have been shown to reliably approximate time-integrated activity estimates from other curve fitting techniques when compared both at the voxel and organ level.

It has been consistently reported that delayed image acquisitions are most important to accurately estimate dosimetry in ¹⁷⁷Lu therapies even for complex pharmacokinetic models.^{28,29} The algorithm in this work is designed to yield curves which pass through the final acquisition time and, where appropriate, will directly determine late-phase clearance based on the line of slope between the second

TABLE II. Median voxel-level error as relative percentage at each of the three imaging time points. Note that the iterative solving method [voxel-based multimodal method (VoMM)] is biased toward reducing error at early images as when activity and associated calculation of residual error would be greatest. The proposed tri-exponential algorithm prioritizes accuracy for the second and third measurements with consideration of the late-phase influence on the estimated time integral.

| Region | 4h | | 24h | | 72h | |
|-----------------------|-----------------|-------|-----------------|-------|-----------------|-------|
| | Tri-exponential | VoMM | Tri-exponential | VoMM | Tri-exponential | VoMM |
| Marrow | 5.0% | 1.4% | 10.3% | 7.4% | 0.0% | 12.2% |
| Muscle | 3.8% | 0.5% | 8.2% | 3.9% | 0.0% | 11.7% |
| Lung | 8.4% | 0.1% | 5.7% | 1.2% | 0.0% | 9.3% |
| Heart | 5.5% | 0.1% | 4.9% | 1.1% | 0.0% | 9.2% |
| Stomach | 8.5% | 4.7% | 6.3% | 7.2% | 0.2% | 7.1% |
| Small bowel | 12.5% | 1.9% | 7.6% | 7.5% | 0.2% | 14.8% |
| Liver | 3.2% | 0.4% | 1.9% | 1.4% | 0.1% | 2.5% |
| Pancreas | 5.7% | 4.5% | 12.1% | 7.2% | 0.1% | 7.9% |
| Spleen | 4.2% | 1.1% | 2.8% | 3.4% | 0.1% | 6.2% |
| Right kidney | 4.3% | 0.5% | 1.3% | 2.3% | 0.1% | 13.8% |
| Left kidney | 4.2% | 0.6% | 1.6% | 2.7% | 0.0% | 14.6% |
| Bladder | 7.2% | 0.0% | 1.9% | 0.6% | 0.0% | 51.2% |
| Lower large intestine | 77.0% | 13.7% | 3.6% | 13.4% | 0.1% | 10.0% |
| Upper large intestine | 21.4% | 5.9% | 2.2% | 8.0% | 0.2% | 16.7% |
| Tumor | 15.9% | 4.7% | 8.5% | 7.3% | 0.3% | 15.2% |

and third image acquisitions. This is in contrast to most iterative least-squares solvers which, in the ordinary case, will be weighted toward uptake when activity is largest, typically at the earliest time point and may be at the expense of accurately characterizing time-integrated activity. This can be improved upon by modifying the objective function to bias the weighting of certain measurements either explicitly or through additional iterative operations,³⁰ but this presents a different set of challenges if the aim is to implement as a general purpose tool to efficiently run in the image space. Balancing patient convenience with quantitative accuracy and ease of use is a motivation for improved algorithms for clinical dosimetry.

There are intrinsic limitations to fitting a six-variable equation to three measured data points; or effectively four if directed through zero at the origin and generic uptake rates are considered. Even with well-conditioned data, the combination of clearance half-times and fractions may be modified to yield an infinite number of solutions which pass through the measurement values. This is constrained if each phase of the multiexponential term depletes to very near zero as it transitions from one measurement to the next. Subsequently, the shape of the curve is influenced by the selection of image times as the inflection between phases 2 and 3 will necessarily occur at the second measurement time. If the time points are not chosen sensibly, or there are inconsistencies in the image times between patients within a cohort, systematic bias could result. This, however, is a challenge for any pharmacokinetic assessment methodology and it is worthwhile to restate the importance of judicious selection of measurements with consideration of the pharmacokinetics and physical half-life of any radiopharmaceutical. Of specific note, when using short half-life isotopes or imaging in the first 2 hours of administration, it is advisable to experiment with the standard uptake rate coefficient, k_1 , which may be modified (and likely reduced) to reliably model the underlying physiology. As with the selection of uptake half-time, the use of conditional assumptions may warrant special consideration for the pharmacokinetics of individual tracers with ^{124}I , ^{131}I , and ^{90}Y being of particular interest in the context of current therapeutic radionuclides. Additionally, with increasing focus on the potential for theranostic isotope pairs such as $^{86}\text{Y}/^{90}\text{Y}$, $^{44}\text{Sc}/^{47}\text{Sc}$, or $^{64}\text{Cu}/^{67}\text{Cu}$ which permit delayed, high-resolution imaging and treatment with an equivalent molecular species, the ability to assess pharmacokinetics in the image space is particularly relevant.

In this report, a working version of the algorithm is distributed as open-source software, which may be employed directly or improved upon by contributing researchers. Because the algorithm runs with a set of conditional statements and a sequence for solving for exponential slope between two points, it is possible to implement in software that handles basic conditional and mathematical operations. For demonstration or use as a region-based dosimetry tool, the algorithm has been incorporated into an interactive spreadsheet, which is available in the supplementary material supporting this article or at the primary author's Github repository.³¹

5. CONCLUSIONS

This report presents a generalizable algorithm to derive time-activity curves from limited temporal measurement data. The methodology relies on separating the curve fitting challenge into piecewise phases similarly to a residual stripping technique. Conditional statements allow the process to be applied in a predictable manner that achieves a sensible compromise in error for voxels which may be subject to noise or inconsistent coregistration. The technique is computationally efficient allowing use for routine image-based dosimetry. A complete version of the algorithm is provided as open-source computer code for developers of nuclear medicine analysis software.

ACKNOWLEDGMENTS

PJ is supported by a Victorian Cancer Agency clinical fellowship. Initial clinical data provided through grant support by the Victorian Cancer Agency clinical trial, "GaTate-PET/CT to predict LuTate dosimetry in patients with neuroendocrine tumour disease: a pilot study" (CI RJH). MSH is supported by a Clinical Fellowship Award from the Peter MacCallum Foundation and receives grants from the Prostate Cancer Foundation (PCF), November, U.S. Department of Defence and the Prostate Cancer Foundation of Australia. He also receives research funding from Advanced Accelerator Applications (a Novartis company). GK is supported by a Clinical Fellowship Award from the Peter MacCallum Foundation. RJH is recipient of a National Health and Medical Research Council Practitioner Fellowship (APP1108050). The authors thank David Sarrut for his advice and input in evaluating the methodology in comparison to his previously published technique.

CONFLICT OF INTEREST

The authors have no conflict to disclose.

^{a)}Author to whom correspondence should be addressed. Electronic mail: price.jackson@petermac.org.

REFERENCES

1. Fanti S, Minozzi S, Antoch G, et al. Consensus on molecular imaging and theranostics in prostate cancer. *Lancet Oncol.* 2018;19:e696–e708.
2. Kwekkeboom DJ, Krenning EP, Lebtahi R, et al. ENETS consensus guidelines for the standards of care in neuroendocrine tumors: peptide receptor radionuclide therapy with radiolabeled somatostatin analogs. *Neuroendocrinology.* 2009;90:220–226.
3. Bolch WE, Bouchet LG, Robertson JS, et al. MIRD pamphlet no. 17: the dosimetry of nonuniform activity distributions—radionuclide S values at the voxel level. *J Nucl Med.* 1999;40:11S–36S.
4. Lanconelli N, Pacilio M, Meo SL, et al. A free database of radionuclide voxel S values for the dosimetry of nonuniform activity distributions. *Phys Med Biol.* 2012;57:517.
5. Dieudonné A, Hobbs RF, Bolch WE, Sgouros G, Gardin I. Fine-resolution voxel S values for constructing absorbed dose distributions at variable voxel size. *J Nucl Med.* 2010;51:1600–1607.
6. Pacilio M, Lanconelli N, Lo Meo S, et al. Differences among Monte Carlo codes in the calculations of voxel values for radionuclide targeted

- therapy and analysis of their impact on absorbed dose evaluations. *Med Phys.* 2009;36:1543–1552.
7. Jackson PA, Hickson K. Integration of GATE Monte Carlo-based radionuclide dosimetry as a practical on-line clinical tool. Paper presented at: 2017 Geant4 User Workshop 2017; University of Wollongong, Wollongong, Australia.
 8. Pacilio M, Amato E, Lanconelli N, et al. Differences in 3D dose distributions due to calculation method of voxel S-values and the influence of image blurring in SPECT. *Phys Med Biol.* 2015;60:1945.
 9. Sgouros G, Frey E, Wahl R, He B, Prideaux A, Hobbs R. Three-dimensional imaging-based radiobiological dosimetry. *Sem Nucl Med.* 2008;38:321–334.
 10. Dewaraja YK, Frey EC, Sgouros G, et al. MIRD pamphlet no. 23: quantitative SPECT for patient-specific 3-dimensional dosimetry in internal radionuclide therapy. *J Nucl Med.* 2012;53:1310–1325.
 11. Ljungberg M, Celler A, Konijnenberg MW, Eckerman KF, Dewaraja YK, Sjögreen-Gleisner K. MIRD pamphlet no. 26: joint EANM/MIRD guidelines for quantitative ^{177}Lu SPECT applied for dosimetry of radio-pharmaceutical therapy. *J Nucl Med.* 2016;57:151–162.
 12. Sarrut D, Halty A, Badel JN, Ferrer L, Bardiès M. Voxel-based multi-model fitting method for modeling time activity curves in SPECT images. *Med Phys.* 2017;44:6280–6288.
 13. Kletting P, Schimmel S, Kestler H, et al. Molecular radiotherapy: the NUKFIT software for calculating the time-integrated activity coefficient. *Med Phys.* 2013;40:102504.
 14. Jackson PA, Beauregard JM, Hofman MS, Kron T, Hogg A, Hicks RJ. An automated voxelized dosimetry tool for radionuclide therapy based on serial quantitative SPECT/CT imaging. *Med Phys.* 2013;40:112503.
 15. Violet J, Jackson P, Ferdinandus J, et al. Dosimetry of ^{177}Lu -PSMA-617 in metastatic castration-resistant prostate cancer: correlations between pretherapeutic imaging and whole-body tumor dosimetry with treatment outcomes. *J Nucl Med.* 2019;60:517–523.
 16. Kirkup L, Sutherland J. Curve stripping and nonlinear fitting of polyexponential functions to data using a microcomputer. *Comput Phys.* 1988;2:64–68.
 17. Siegel JA, Thomas SR, Stubbs JB, et al. MIRD pamphlet no. 16: techniques for quantitative radiopharmaceutical biodistribution data acquisition and analysis for use in human radiation dose estimates. *J Nucl Med.* 1999;40:37S–61S.
 18. Stabin M, Xu XG. Basic principles in the radiation dosimetry of nuclear medicine. *Sem Nucl Med.* 2014;44:162–171.
 19. Stabin MG, Sparks RB, Crowe E. OLINDA/EXM: the second-generation personal computer software for internal dose assessment in nuclear medicine. *J Nucl Med.* 2005;46:1023–1027.
 20. Grassi E, Fioroni F, Ferri V, et al. Quantitative comparison between the commercial software STRATOS® by Philips and a homemade software for voxel-dosimetry in radiopeptide therapy. *Physica Med.* 2015;31:72–79.
 21. Virtanen P, Gommers R, Oliphant TE, et al. SciPy 1.0: fundamental algorithms for scientific computing in Python. *Nat Methods.* 2020;1–12.
 22. Van Der Walt S, Colbert SC, Varoquaux G. The NumPy array: a structure for efficient numerical computation. *Comput Sci Eng.* 2011;13:22.
 23. Klein S, Staring M, Murphy K, Viergever MA, Pluim JP. Elastix: a toolbox for intensity-based medical image registration. *IEEE Trans Med Imaging.* 2010;29:196–205.
 24. Willowson KP, Ryu H, Jackson P, Singh A, Eslick E, Bailey DL. A comparison of 2D and 3D kidney absorbed dose measures in patients receiving ^{177}Lu -DOTATATE. *Asia Ocean J Nucl Med Biol.* 2018;6:113.
 25. Hicks RJ, Jackson P, Kong G, et al. First-in-human trial of ^{64}Cu -SAR-TATE PET imaging of patients with neuroendocrine tumours demonstrates high tumor uptake and retention, potentially allowing prospective dosimetry for peptide receptor radionuclide therapy. *J Nucl Med.* 2018;60:777–785.
 26. Pattison DA, Solomon B, Hicks RJ. A new theranostic paradigm for advanced thyroid cancer. *J Nucl Med.* 2016;57:1493–1494.
 27. Kong G, Callahan J, Hofman MS, et al. High clinical and morphologic response using ^{90}Y -DOTA-octreotate sequenced with ^{177}Lu -DOTA-octreotate induction peptide receptor chemoradionuclide therapy (PRCRT) for bulky neuroendocrine tumours. *Eur J Nucl Med Mol Imaging.* 2017;44:476–489.
 28. Hänscheid H, Lapa C, Buck AK, Lassmann M, Werner RA. Absorbed dose estimates from a single measurement one to three days after the

administration of ^{177}Lu -DOTATATE/TOC. *Nuklearmedizin.* 2017;56:219–224.

29. Madsen MT, Menda Y, O'Dorisio TM, O'Dorisio MS. Single time point dose estimate for exponential clearance. *Med Phys.* 2018;45:2318–2324.
30. Muzic RF Jr., Christian BT. Evaluation of objective functions for estimation of kinetic parameters. *Med Phys.* 2006;33:342–353.
31. Jackson PA. Github - TriExponential-Solver; 2019. <https://github.com/jacksonmedphysics/TriExponential-Solver>

SUPPORTING INFORMATION

Additional supporting information may be found online in the Supporting Information section at the end of the article.

Fig. S1. Time-activity curve approximated for data with greatest uptake measured at the final time point c_3 . Physical decay is assumed beyond and a single uptake phase may be used to approximate the kinetics between $t = 0$ and c_3 . Dotted line represents the late-phase retention beyond c_3 . On right plot, separate phases are plotted individually; uptake phase shown as dashed line. The resulting time-activity curve is shown as solid line against measured values on left.

Fig. S2. Example of serial activity measurements requiring conditional adjustment to solve analytical time-activity curve. This may occur due to image alignment issues or noise and is unlikely to represent true physiology. Here the activity declines at c_2 and increases again at c_3 . This may be detected by conditional statement and the measurement c_2 is adjusted to match the slope for very near physical clearance between time points c_2 and c_3 . The piecewise solving process may then proceed as normal.

Fig. S3. A second pattern of measurement that may be detected by conditional statement. By first shifting the measured activity at c_2 to the linear interpolation between c^1 and c_3 , solving with the piecewise algorithm approximates the behavior of a least-squares optimizer, yielding a curve that is a compromise of early measured data.

Fig. S4. Initial preconditioning of values with very low measurements relative to the second time point. These tend to occur in low-uptake regions or where there are errors in image alignment and this may prevent calculation of very large exponential decay slopes.

Fig. S5. Calculation of comparison values c_2 , plateau and c_2 , linear which may be employed to handle unrealistic cases (e.g., high-low-high uptake).

Fig. S6. Primary flowchart for solving time-activity curve as a two- or three-phase exponential decay curve. Note: the common case with one uptake phase and two separate clearance components is denoted in bold.

Table S1. Effect on estimated time-integrated activity of changing generic uptake rate parameter, k_1 . Difference is reported as a percentage relative the 30 minute half-time used elsewhere for analysis. For the majority of regions and all long-retaining tissues in particular, the time integral is insensitive to the selection of rate parameter with a typical variation less than 2% for values selected between 20 and 90 minutes.